Journal of Computational Physics **172,** 808–826 (2001)
doi:10.1006/jcph.2001.6859, available online at http://www.idealibrary.com on IDEAL®

The Euler Equations for Multiphase Compressible Flow in Conservation Form

Simulation of Shock–Bubble Interactions

Robin K. S. Hankin

School of Environmental and Marine Sciences, University of Auckland, Morrin Road, Building 733, Private Bag 92109, Glenn Innes, Auckland, New Zealand
E-mail: r.hankin@auckland.ac.nz

Received October 17, 2000; revised June 20, 2001

The Euler equations, together with an equation of state, govern the motion of an inviscid compressible fluid. Here, a new equation of state for volumes containing both gas and liquid is derived; this allows the Euler equations for two substances, here air and water, to be expressed in pure conservation form. This in turn allows simulation of shocks in water interacting with small bubbles of air as the meniscus no longer needs to be tracked explicitly. Extension to three space dimensions is shown to be straightforward.

A test case showing how a shock wave in water interacts with a small (two-dimensional) air bubble is presented. Simulations of a shock wave interacting with two air bubbles, and a small multiphase region (comprising 50% water and 50% air by volume) are then given.

Key Words: Euler equations; shocks; compressible gas flow; equation of state.

1. INTRODUCTION

All fluids admit some compressibility and therefore support shock waves. A shock wave is an abrupt (Lagrangian) change in fluid density and velocity; shock waves are thermodynamically irreversible and, in the cases considered here, are of negligible thickness.

Shock waves may be produced in liquids such as seawater by a variety of natural and artificial mechanisms [14]. Also, shock waves may be produced in human tissue in the process of shock wave lithotripsy [19]. Here, shock waves are produced in water at one focus of an ellipsoidal tank. Shock waves pass almost unaltered into the patient, and (say) a kidney stone at the other focus will receive concentrated sonic energy, causing disintegration.

0021-9991/01 $35.00

The methods presented here are also of relevance to the study of shock wave propagation in a bubbly liquid [16]; and the equation of state presented in the present work is directly applicable to liquid explosives with gas cavities [2, 5, 32]. Tan and Bankoff [30] consider shock waves propagating through dilute bubbly mixtures but assume that the liquid phase is incompressible, and that the bubbles remain spherical.

In these applications, it is important and interesting to understand the behavior of a shock wave when it interacts with a small air bubble; for example, Delius *et al*. [6] considered lithotripsy *in vitro* and concluded that the dominant mechanism of shock wave action on cells is shock wave–gas bubble interaction.

When considering shock wave–gas bubble interaction, complications are introduced by having two separate equations of state [8, 26]. To date, only limited success with this problem in more than one space dimension has been achieved, although Ding and Gracewski [7], Ivings [14], and Grove and Menikoff [9] have applied adaptive mesh techniques to similar cases (these workers' simulations did not continue after the shock had passed the bubble).

Here, a technique is presented that overcomes many of the disadvantages of adaptive meshes in a computationally cheap manner. A new equation of state for gas–water mixtures is derived that allows simulation of a wide range of two-phase flows including bubbly fluids [20], fogs [24], and foams [23].

The present work builds upon that of Saurel and Abgrall [26, 27], and Grove and Menikoff [9], by presenting the Euler equations in conservation form. This allows simulations to be carried out in two or three space dimensions, although only two-dimensional problems are considered here.

Several test cases are presented. A detailed simulation of a shock–bubble interaction is given, followed by a shock wave interacting with a system of two closely separated bubbles, and a region comprising 50% water and 50% air by volume.

2. THE EULER EQUATIONS

The Euler equations in two dimensions are

$$\frac{\partial \rho}{\partial t} + \frac{\partial \rho u}{\partial x} + \frac{\partial \rho v}{\partial y} = 0 \tag{1}$$

$$\frac{\partial \rho u}{\partial t} + \frac{\partial \rho u^2}{\partial x} + \frac{\partial \rho uv}{\partial y} + \frac{\partial p}{\partial x} = 0 \tag{2}$$

$$\frac{\partial \rho v}{\partial t} + \frac{\partial \rho uv}{\partial x} + \frac{\partial \rho v^2}{\partial y} + \frac{\partial p}{\partial y} = 0 \tag{3}$$

$$\frac{\partial E}{\partial t} + \frac{\partial u(E+p)}{\partial x} + \frac{\partial v(E+p)}{\partial y} = 0, \tag{4}$$

where ρ is the density, $\mathbf{u} = (u, v)$ the velocity, E the stagnation energy per unit volume, and p the pressure of the fluid. The pressure may be specified by the equation of state. Here, the Tammann (or stiffened) equation of state [21] is used, following Grove and Menikoff [9], and Saurel and Abgrall [27]:

$$p = \rho(\gamma - 1)e - \gamma p^0, \tag{5}$$

where γ is the adiabatic exponent [21], $e = E/\rho - \frac{1}{2}(u^2 + v^2)$ is the internal energy per unit mass, and p^0 a substance-specific pressure adjustment term that accounts for the short-range attraction between liquid molecules. For water, $p^0 \simeq 3 \times 10^8$ Pa [9]; and for air $p^0 = 0$ taken to be an ideal gas—Eq. 5 thereby reducing to the ideal gas law. Here, $\gamma = 1.4$ is used for air, and the experimentally determined value of 7.15 is used for water.

Simulation of these equations in two and three dimensions, in a single medium, has received much attention; Woodward and Colella [33] give a review article.

However, if two separate substances are considered, Eqs. 1 to 5 must be augmented to keep track of the fluid properties γ and p^0. Because these quantities are advected (that is, $\partial\gamma/\partial t + \mathbf{u} \cdot \boldsymbol{\nabla}\gamma = 0$) then Eq. 1 shows

$$\frac{\partial \rho\gamma}{\partial t} + \frac{\partial \rho\gamma u}{\partial x} + \frac{\partial \rho\gamma v}{\partial y} = 0 \tag{6}$$

$$\frac{\partial \rho p^0}{\partial t} + \frac{\partial \rho p^0 u}{\partial x} + \frac{\partial \rho p^0 v}{\partial y} = 0. \tag{7}$$

2.1. Euler Equations and Multiple Equations of State

Equations 1 to 7 allow simulation of a shock travelling through an air–water interface. However, in practice, the equation of state (henceforth EOS) is poorly behaved when air–water mixtures are considered.

Ivings [14] considered a volume V at pressure p, comprising νV water (substance 1, density ρ_1) and $(1-\nu)V$ air (substance 2, density ρ_2). The density is $\nu\rho_1 + (1-\nu)\rho_2$ by definition, and a representative adiabatic exponent γ was given by Ivings as

$$\gamma = \nu\gamma_1 + (1-\nu)\gamma_2 \tag{8}$$

because γ is advected, not conserved. Similar interpolations give the other advected terms; Ivings then used the EOS (Eq. 5) to give an expression algebraically equivalent to

$$p = \underbrace{(\nu\rho_1 e_1 + (1-\nu)\rho_2 e_2)}_{\overline{\rho e}} \cdot \underbrace{(\nu\gamma_1 + (1-\nu)\gamma_2 - 1)}_{\bar{\gamma}-1} - \underbrace{(\nu\gamma_1 p^0 + (1-\nu)\cdot 0)}_{\overline{\gamma p^0}}, \tag{9}$$

and noted that this approach is defective in the sense that the EOS given by Eq. 9 predicts that p is a function of ν when applied to a control volume containing water and air both at pressure p. Ivings showed that this expression gives negative pressures for most values of ν with $0 \leqslant \nu \leqslant 1$. Shyue [28] presents a slightly different technique, generalized for an arbitrary number of phases.

Ivings considered that the failure to predict a constant pressure p was a failure of conservative numerical methods; Ton [31] attributes this failure to a "failure of thermodynamic consistency in the EOS in cells containing [more than one] species." Here it is shown that conservative methods may indeed be used if a different EOS is adopted.

The pathology of nonconstant p prompted Ivings [14] to consider air–water shock interactions in terms of two separate computational regions with a line, representing the meniscus, separating them (only two space dimensions were considered). This approach suffers from a number of disadvantages, one of which is the difficulty of testing for changes in topology of the meniscus: in two dimensions, a bubble has a meniscus that is a circle,

whereas during many shock–bubble interactions the meniscus separates into two separate regions. Dealing with this type of behavior is difficult [10] in two dimensions, and has no obvious generalization to three dimensions.

Note that there are two distinct types of discontinuity to consider: a discontinuity of phase—here the meniscus—and a discontinuity of density within one substance such as a shock front. Thus, considerations of modelling the meniscus may be different from those governing choice of shock-tracing methods or shock-smearing methods [25].[1] For example, Ivings used shock-smearing methods for the shock front together with an explicit discontinuity—the meniscus—separating the two phases. Mulder *et al.* [22] discuss the problem of interface motion in a more general context.

3. EQUATION OF STATE FOR MIXTURES

3.1. Overview

Consider a volume containing gaseous air and liquid water at the same temperature and an unknown pressure p. It is clear that volume fraction ν of water is a function of p (in general, ν is an increasing function of pressure).

In typical compressible flow situations, a small computational fluid element of volume V is considered that possesses known internal energy ρeV, and a known mass of air and water ($\rho_1 V$ and $\rho_2 V$, respectively). A meniscus will separate two phases obeying qualitatively different equations of state.

It is shown in this paper that the two equations furnished by equality of temperature and pressure across the meniscus will determine the unknown values of pressure p and volume fraction ν.

In particular, determination of the pressure within the control volume is an EOS for mixtures; this allows solution of the Euler equations in conservation form.

3.2. Densities and Conserved Quantities

The EOS applied to a volume containing water and air fails because it effectively assumes homogeneity; whereas in reality any control volume containing air and water has two distinct phases, separated by a meniscus.

It is possible to proceed by applying the EOS to each phase separately and using the fact that the pressure in each phase is identical. We again consider a volume V comprising νV substance 1 (water) and $(1-\nu)V$ substance 2 (air).

Rather than conserve total mass and keep track of substance properties (Eqs. 1, 6, and 7) it is possible to conserve the amount of each substance explicitly. This approach requires the introduction of two further conserved variables, ρ_1 and ρ_2, representing the densities of substances 1 and 2, respectively. These quantities are mass (of substance 1 and 2) per unit volume, and are therefore conserved:

$$\frac{\partial \rho_1}{\partial t} + \frac{\partial \rho_1 u}{\partial x} + \frac{\partial \rho_1 v}{\partial y} = 0 \tag{10}$$

[1] In the shock tracing approach, a discontinuity is maintained explicitly; the shock-smearing approach models a discontinuity as spread over a small number of computational elements. Here, shock-smearing techniques are used to cover both the shock and the meniscus. Shock-smearing methods are generally preferable in this type of application as they can more easily accommodate changes in genus.

$$\frac{\partial \rho_2}{\partial t} + \frac{\partial \rho_2 u}{\partial x} + \frac{\partial \rho_2 v}{\partial y} = 0. \tag{11}$$

Equations 10 and 11 refer to densities that are mass of substance per unit volume. Now the EOS requires densities of a different character from ρ_1 and ρ_2 of Eqs. 10 and 11: the density required by an EOS is mass of substance per unit volume *of that substance*. Densities thus defined (i.e., mass of substance per unit volume of that substance) are not conserved in the sense that they do not obey a conservation equation such as Eq. 10. Such densities will henceforth be distinguished from conserved densities by the superscript "r," as in ρ_1^{r}.

3.3. EOSs for the Separate Phases

There are two EOSs for the volume, one for substance 1 and one for substance 2,

$$p = \rho_1^{\mathrm{r}}(\gamma_1 - 1)e_1^{\mathrm{r}} - \gamma_1 p^0 \tag{12}$$

$$= \rho_2^{\mathrm{r}}(\gamma_2 - 1)e_2^{\mathrm{r}}, \tag{13}$$

where the superscript "r" in e_1^{r} means "internal energy per unit mass of substance 1" and similarly for e_2^{r}. Now $\rho_1^{\mathrm{r}} = \rho_1/\nu$ and $\rho_2^{\mathrm{r}} = \rho_2/(1-\nu)$; and $e_1^{\mathrm{r}} = e_1 \frac{\rho}{\rho_1}$ and $e_2^{\mathrm{r}} = e_2 \frac{\rho}{\rho_2}$.

3.4. Equality of Pressures

Using the fact that the pressures of the two phases are identical (Eqs. 12 and 13) gives an equation for ν,

$$\frac{\rho}{\nu}(\gamma_1 - 1)e_1 - \gamma_1 p^0 = \frac{\rho}{1-\nu}(\gamma_2 - 1)e_2, \tag{14}$$

where $\rho_i^{\mathrm{r}} e_i^{\mathrm{r}}$ has been rewritten in terms of ρe and ν (if $\nu = 0$ or 1 exactly then the problem reduces to the single substance case).

This approach differs from that of Saurel and Abgrall [26], who consider a mixture pressure P defined (in the current notation) by $P = \nu p_1 + (1-\nu)p_2$, where p_i is the pressure of fluid i. Their approach is not applicable in the current context because phase 1 (water) is unstable to condensation unless ν is very close to unity.

3.5. Internal Energies

Equation 14 has three unknowns: ν, e_1, and e_2. In order to close the system, another relationship is required in addition to the requirement that $e = e_1 + e_2$. There are two ways to proceed: the temperature across the meniscus may be assumed to be constant; or, following Saurel and Abgrall [26], the two phases may be allowed to have different temperatures.

Both approaches are described mathematically below and discussed further in Section 4.1.

3.6. Equation of State for Gas–Water Mixtures at Equal Temperatures

The kinetic theory of gases implies

$$T_2 = (\gamma_2 - 1)e_2^{\mathrm{r}}/R, \tag{15}$$

assuming air to be a polytropic gas. Here, T_2 is the thermodynamic temperature of air in Kelvin, and R is the gas constant, here taken to be 479 $\mathrm{Pa}\cdot\mathrm{m}^3\cdot\mathrm{kg}^{-1}\,\mathrm{K}^{-1}$. The Tammann EOS implies

$$T_1 = \frac{(\gamma_1 - 1)\left(\rho_1^{\mathrm{r}} e_1^{\mathrm{r}} - p^0\right)}{\rho_1^{\mathrm{r}} K}, \tag{16}$$

where K is the liquid constant; following Sugimura *et al.* [29], this is taken to be 1089 $\mathrm{Pa}\cdot\mathrm{m}^3\cdot\,\mathrm{kg}^{-1}\,\mathrm{K}^{-1}$. Equality of temperatures gives an equation linking ν with e_1 and e_2,

$$\frac{\gamma_1 - 1}{K} \cdot \frac{\rho e_1 - \nu p^0}{\rho_1} = \frac{\gamma_2 - 1}{R} \cdot \frac{\rho e_2}{\rho_2}, \tag{17}$$

where the above definitions for ρ_i^{r} and e_i^{r} have been used. Equation 17 now gives

$$e_1 = \frac{e c_2 \rho_1 + \nu(p^0/\rho) c_1 \rho_2}{c_2\rho_1 + c_1\rho_2} \tag{18}$$

$$e_2 = \frac{e c_1 \rho_2 - \nu(p^0/\rho) c_1 \rho_2}{c_2\rho_1 + c_1\rho_2}, \tag{19}$$

where $c_1 = (\gamma_1 - 1)/K$ and $c_2 = (\gamma_2 - 1)/R$. Some implications of the assumption of thermal equilibrium are discussed below in Section 4.1. Substituting Eqs. 18 and 19 into 14 gives, after simplification,

$$\begin{aligned} f(\nu) &= \nu^2(c_1\rho_2\gamma_2 p^0 + c_2\rho_1\gamma_1 p^0) - \nu[\rho e(c_2\rho_1(\gamma_1 - 1) + c_1\rho_2(\gamma_2 - 1)) \\ &\quad + (c_1\rho_2\gamma_2 p^0 + c_2\rho_1\gamma_1 p^0)] + \rho e c_2\rho_1(\gamma_1 - 1) \\ &= 0. \end{aligned} \tag{20}$$

Equation 20 has a root in the interval $[0, 1]$ because f is continuous and $f(1) \leqslant 0 \leqslant f(0)$; the root is unique because f' is strictly monotonic (the case $f(0) = f(1) = 0$ is forbidden if $\rho > 0$); and it has the required properties when ρ_1 or $\rho_2 = 0$. The meaningful root is the smaller of the two because we require $0 \leqslant \nu \leqslant 1$ and the larger root is always >1 (the coefficient of ν^2 is positive). Solving Eq. 20 for ν and substituting into Eq. 13 gives, if $\rho_1 \neq 0$,

$$p = -\gamma_1 p^0 + \frac{\rho(\gamma_1 - 1)}{\nu} \cdot \frac{e c_2\rho_1 + \nu(p^0/\rho) c_1\rho_2}{c_2\rho_1 + c_1\rho_2} \tag{21}$$

where $$\nu = \frac{b - \sqrt{b^2 - 4ac}}{2a}$$

and
$$a = c_1\rho_2\gamma_2 p^0 + c_2\rho_1\gamma_1 p^0$$
$$b = \rho e(c_2\rho_1(\gamma_1 - 1) + c_1\rho_2(\gamma_2 - 1)) + c_1\rho_2\gamma_2 p^0 + c_2\rho_1\gamma_1 p^0$$
$$c = \rho e c_2\rho_1(\gamma_1 - 1).$$

If $\rho_1 = 0$ then the limit is correct; alternatively the right hand side of equation 14 gives the appropriate general expression. It may be verified directly that equation 21 behaves as expected when either ρ_1 or $\rho_2 = 0$.

3.6.1. *Equation of State for Gas–Water Mixtures at Unequal Temperatures*

It is instructive to consider how Eqs. 1 to 4 and the isothermal EOS have to be changed to accommodate the extra degree of freedom introduced by allowing the phases to have different temperatures. The resulting equations are not solved here.

The EOS (Eq. 21) assumed that both phases were at the same temperature; relaxing this assumption requires new equations for the internal energy of each phase separately. Because Eq. 4 governs only the total stagnation energy per unit volume, a new equation is required to keep track of the stagnation energies of the two phases separately.

Following Saurel and Abgrall [26] (but adopting the current approach of a unique pressure and velocity at any point), the relevant equations are

$$\frac{\partial E_1}{\partial t} + \frac{\partial u(E_1 + \nu p)}{\partial x} + \frac{\partial v(E_1 + \nu p)}{\partial y} = -p\frac{\partial \nu}{\partial t} \tag{22}$$

$$\frac{\partial E_2}{\partial t} + \frac{\partial u(E_2 + (1-\nu) p)}{\partial x} + \frac{\partial v(E_2 + (1-\nu) p)}{\partial y} = +p\frac{\partial \nu}{\partial t}, \tag{23}$$

where $E_1 = \rho e_1 + \frac{1}{2}\rho_1(u^2 + v^2)$ and $E_2 = \rho e_2 + \frac{1}{2}\rho_2(u^2 + v^2)$ are the stagnation energies per unit volume for each phase; adding Eqs. 22 to 23 recovers conservation of total energy. The nonconservative terms on the right-hand side correspond to the phases doing work on one another when the volume fraction changes.

Equations 22 and 23 do not imply independence of the two phases; both move at the same velocity, and the phases may exchange energy mechanically.

If the internal energies of the two phases are known, Eq. 14 gives

$$f(\nu) = \nu^2 - \nu[\alpha_1(\gamma_1 - 1) + \alpha_2(\gamma_2 - 1) + 1] + \alpha_1(\gamma_1 - 1) = 0, \tag{24}$$

where $\alpha_1 = \rho e_1/(\gamma_1 p^0)$ and $\alpha_2 = \rho e_2/(\gamma_1 p^0)$ are nondimensionalized internal energies. Again a root with $0 \leqslant \nu \leqslant 1$ is required. As for Eq. 20, such a root exists and is the smaller of the two solutions. Substituting the appropriate solution to Eq. 24 into Eq. 14 gives

$$p = \begin{cases} -\gamma_1 p_1^0 + \frac{2\rho e_1(\gamma_1 - 1)}{b - \sqrt{b^2 - 4c}}, & \text{if } \rho_1 \neq 0 \\ \frac{2\rho(\gamma_2 - 1)e_2}{2 + b + \sqrt{b^2 - 4c}}, & \text{if } \rho_2 \neq 0, \end{cases} \tag{25}$$

where $-b = \alpha_1(\gamma_1 - 1) + \alpha_2(\gamma_2 - 1) + 1$ and $c = \alpha_1(\gamma_1 - 1)$ are the second and third coefficients in Eq. 24. Equations 25 require two different forms to handle the limiting cases of $\rho_1 = 0$ and $\rho_2 = 0$, because vanishing density does not imply vanishing internal energy. This issue does not arise for the isothermal case.

3.7. Summary

The EOS is applied to each phase separately. The two EOSs use densities ρ_i^{r}—defined as mass of phase i per unit volume of that phase (thus implicitly recognizing the presence of a meniscus)—and internal energy densities e_i^{r}, defined as internal energy per unit mass of

phase i. The two unknowns—pressure p and volume fraction ν—are determined in terms of the conserved variables in two different ways depending on whether the phases are assumed to be the same temperature.

In the isothermal case, the two required equations are obtained by matching pressure and temperature across the meniscus. The resulting EOS is applicable to an isothermal air–water mixture.

If differing temperatures across the meniscus are allowed, as discussed by Saurel and Abgrall [26], the internal energies of each phase have to be obtained from two energy conservation equations, one for each phase. The remaining unknown is furnished by the equality of pressures on either side of the meniscus.

The isothermal EOS presented here allows simulation of the Euler equations in conservation form.

4. APPLICATIONS FOR A MIXTURE EOS

Equation 21, although designed for control volumes through which a single meniscus passes, is applicable to any volume containing water and air at the same temperature.

In particular, strong shock waves through air–water foams, bubbly fluid, or air laden with water droplets may be simulated using Eq. 21 as an EOS, following Saurel and Abgrall [26]. These workers maintain a terminological distinction between multiphase and multifluid flows: multiphase flows have many interfaces which are not tracked individually, whereas in multifluid flows, most of the control volumes contain pure phases and the interfaces are well-defined.

The related problem of compressible flow in a dust-laden gas [3, 24] has received much attention under the assumption that the second phase (dust) is incompressible. The present work, in contrast, allows for the compressibility of the nongaseous fraction; equivalently, the restriction to pressure $\ll \gamma_1 p^0$ is relaxed.

Young [34] considers droplet-laden flow, again with the assumption that the nongaseous phase is incompressible. He shows that surface energy terms can be important; but in the present work the Weber number (based on bubble diameter and post-shock fluid speed) is about 10^7, so these effects may be neglected.

In both multiphase and multifluid flows, the EOS is applied to control volumes that may possess a meniscus but may be regarded as homogeneous on the lengthscale of the computational grid. Examples of fluids satisfying this restriction would include droplet-laden air, and bubbly liquids.

Such multiphase flows may have strikingly different properties from single phase fluids. For example, consider water at 2×10^9 Pa and 15°C that includes 1% air by volume (this pressure is approximately that considered in the case study below). If such a two-phase mixture were allowed to expand isothermally to atmospheric pressure, its volume would increase by a factor of about 200—in contrast to pure water at this pressure, which would expand by a factor of about 1.8.

It may be shown that the speed of sound c associated with this EOS obeys

$$c^2 = \frac{\rho_1}{\rho}\frac{\partial p}{\partial \rho_1} + \frac{\rho_2}{\rho}\frac{\partial p}{\partial \rho_2} + \frac{p}{\rho^2}\frac{\partial p}{\partial e}, \tag{26}$$

but the full algebraic form is rather opaque.

4.1. Equality of Temperatures

The EOS 21 essentially assumes equality of temperature across the meniscus: each computational fluid element is at one temperature.

For control volumes with a homogeneous EOS, spatial temperature variation is not an issue because then the pressure is a function only of total internal energy and density. However, as discussed by Jenny *et al*. [15], a closed control volume containing a contact discontinuity separating polytropic gases of identical pressure, but different γ and temperature, does pose problems.

If these two phases are allowed to come to thermal equilibrium a change in pressure occurs, essentially because the specific heat c_V is different in either phase [17, 18].

Although Jenny *et al*. [15] characterize this behavior as an "error," it is possible to consider the change in pressure as a real change resulting from nonzero thermal conductivity. Jenny *et al*. nullified this error by adjusting the total energy per unit volume in such a way as to maintain a constant pressure.

Ton [31], considering mixtures of polytropic gases, states that each species needs to "retain its own properties, especially its temperature." This statement is not applicable to air–water mixtures because Ton effectively assumes $p^0 = 0$ and so the issue of instability to condensation does not arise.

In the present context, in which energy is conserved exactly, it is instructive to consider the effects of the assumption of constant temperature when this may not be the case.

If thermal diffusion is Fickian, the thickness of the thermal boundary layer that develops after time τ is $\sim\sqrt{\tau\kappa}$, where κ is the thermal diffusivity. A reasonable timescale to use would be r/c, where r is the bubble radius and c the speed of sound; this gives a lengthscale l of $\sim 6 \times 10^{-6}$ m. Numerical lengthscales of this order are impractically small for the present case.

However, an estimate for the deviation from the thermally isolated case may be made as follows. For simplicity, only phase 2 (air) is considered, because spurious increases of internal energy in air generate far more mechanical energy. The phase "numerical heat conduction" is used here to mean the difference in internal energy of a phase between its real value ρe_i and the value as calculated on the basis of thermal equilibrium; numerical conduction is thus a phenomenon confined to a single computational element.

If a control volume containing two phases at equal temperature is considered then, using the notation introduced in Section 3, the internal energy in phase 2 is

$$\overline{\rho e_2} = \frac{\left(\nu\rho_1^{\mathrm{r}} + (1-\nu)\rho_2^{\mathrm{r}}\right) \cdot \left(ec_1\rho_2^{\mathrm{r}}(1-\nu) - \nu p^0 c_1 (1-\nu)\rho_2^{\mathrm{r}}\right)}{c_2\rho_1^{\mathrm{r}}\nu + c_1\rho_2^{\mathrm{r}}(1-\nu)}, \tag{27}$$

where Eq. 19 has been used for e_2. In the general case, where the phases are allowed to be at different temperatures, the internal energy is

$$\rho e_2 = (1-\nu)\rho_2^{\mathrm{r}} e_2^{\mathrm{r}}. \tag{28}$$

A measure of the impact of assuming a computational fluid element to be isothermal is given by comparing the difference between expressions (27) and (28) (that is, the energy transferred by numerical heat conduction across the meniscus) and the *mechanical* work done on the second phase.

Taking the least favorable case conceivable (water has an infinite heat capacity compared with that of air; and using e_2^{r} for post-shock water and e_1^{r} for undisturbed air), the internal

energy transferred to phase 1 by numerical conduction is $\sim r\delta x\rho_2^{\mathrm{r}}(e_2 - e_1)$ per unit width; the mechanical work done on the bubble is $\sim r^2 p$ per unit width. Here, δx is the numerical gridsize, and p the post-shock pressure.

The nondimensional ratio $\delta x\rho_2^{\mathrm{r}}(e_2 - e_1)/rp$ is about 3×10^{-6} for the bubble considered in Section 6. The assumption of local thermal equilibrium is thus justified because the bubble receives far more energy through mechanical work than it does from numerical conduction.

4.1.1. *Thermal Equilibrium: Summary*

The above argument showed that the assumption of uniform temperature across a computational grid cell is incompatible with measured thermal diffusivity of air or water.

However, it was then shown that the the mechanical work done on a small bubble (the second test case considered in Section 6) dominated the numerical conduction terms. This is because numerical conduction occurs only over a single computational grid cell.

It should be noted that the system presented here, although it assumes thermal equilibrium within a single grid cell is nevertheless able to simulate non isothermal flow, with the proviso that thermal gradients cannot be resolved at lengthscales $\lesssim \delta x$. For example, in the test case considered in Section 6, the temperatures of the pre- and post- shock fluids differ by about 1148 K and this discontinuity of temperature is resolved to about four or five computational elements.

5. SOLVING THE ADVECTION EQUATION

The advection equations (1) to (4), being in conservation form, are a special case of the general advection equation

$$\frac{\partial w}{\partial t} + \frac{\partial f}{\partial x} + \frac{\partial g}{\partial y} = 0. \tag{29}$$

If we specify

$$w = \begin{pmatrix} \rho_1 \\ \rho_2 \\ \rho u \\ \rho v \\ E \end{pmatrix} \quad f = \begin{pmatrix} \rho_1 u \\ \rho_2 u \\ \rho u^2 + p \\ \rho uv \\ u(E + p) \end{pmatrix} \quad g = \begin{pmatrix} \rho_1 v \\ \rho_2 v \\ \rho uv \\ \rho v^2 + p \\ v(E + p) \end{pmatrix} \tag{30}$$

together with an EOS and the requirement that $\rho = \rho_1 + \rho_2$, then the two-dimensional Euler equations are recovered. One benefit of considering equations in this form is that the components of f and g may be regarded as fluxes; and in the context of numerical techniques the standard format

$$\begin{aligned} w(x, y; t + \delta t) = {} & w(x, y; t) \\ & + (\delta x \delta y)^{-1} \left[f\left(x - \frac{1}{2}\delta x, y; t\right) - f\left(x + \frac{1}{2}\delta x, y; t\right) \right] \delta y \delta t \\ & + (\delta x \delta y)^{-1} \left[g\left(x, y - \frac{1}{2}\delta y; t\right) - g\left(x, y + \frac{1}{2}\delta y; t\right) \right] \delta x \delta t \end{aligned} \tag{31}$$

clearly shows that the components of f and g have the characteristics of fluxes.

Numerical solution of this class of equations is not simple and many numerical schemes have been devised; review articles are given by Chock [4] and Woodward and Colella [33]. The scheme used here is the Flux Corrected Transport (FCT) scheme of Zalesak [35], used without modification.

5.1. The Flux Correction Scheme of Zalesak

FCT calculates the fluxes between adjacent elements by taking a weighted average of the flux as computed by a low-order scheme and the flux as computed by a high-order scheme. The weighting is done in such a manner as to use the high-order scheme unless to do so would result in the creation of overshoots (characterized as new extrema) not predicted by the low-order scheme. The assumption is therefore that any new extrema predicted by the low-order scheme are genuine.

5.1.1. *The Low-Order Convective Flux*

The low-order flux f^L used is simply a donor cell scheme plus a zeroth-order diffusive flux with coefficient D. In one dimension,

$$f^L_{i+(1/2)} = \frac{1}{2}(u_i + u_{i+1}) w^{\mathrm{DC}}_{i+(1/2)} - D\delta x \left(w^n_{i+1} - w^n_i\right)(\Delta t)^{-1}, \tag{32}$$

where

$$w^{\mathrm{DC}}_{i+(1/2)} = \begin{cases} w^n_i & \text{if } u_i + u_{i+1} \geq 0 \\ w^n_{i+1} & \text{if } u_i + u_{i+1} < 0 \end{cases} \tag{33}$$

is read "w donor cell" and u_i is the fluid speed in cell i. Extension to multidimensions is straightforward.

5.1.2. *The High-Order Convective Flux*

The high-order flux f^H used here is taken from a later work by Zalesak [36]. Zalesak called these expressions "high-order ZIP fluxes," following the terminology of Hirt [13]. Zalesak presented a number of theoretical advantages of ZIP fluxes and pointed out that a given order of accuracy was more simply achieved using this scheme. To fourth-order accuracy:

$$f^H_{i+(1/2)} = \frac{2}{3}[w_{i+1}u_i + w_i u_{i+1}] - \frac{1}{12}[w_{i+2}u_i + w_i u_{i+2} + w_{i+1}u_{i-1} + w_{i-1}u_{i+1}]. \tag{34}$$

5.1.3. *Flux Limiting and Conservation Equations*

Zalesak's flux correction scheme has been used by the present author to solve Eq. (29) in the context of heavy gas dispersion [12] modelled using the resisted shallow water equations, and liquid spills [11]. All these systems share with the Euler equations the ability to support discontinuous solutions (i.e., shocks or hydraulic jumps).

The numerical domain used here is a 200×200 grid of computational elements, each 0.15 mm square. The Courant number [25] and the zeroth-order diffusion coefficient [35] were both fixed at 0.1.

The simulations presented here took about 30 minutes on a PC (Pentium III, 450MHz processor).

6. RESULTS: SHOCK–BUBBLE INTERACTION

The above numerical scheme is now used to simulate the Euler equations (29) with the EOS given in Eq. (21). Results are given of a shock interacting with: a one-dimensional bubble; a small two-dimensional (cylindrical) bubble; two bubbles of different sizes; and finally a region comprising 50% water and 50% air.

6.1. Shock–Bubble Interaction: Planar Bubble

The present scheme is now used to simulate a shock interacting with a planar air bubble. The fluid properties and shock characteristics are given in Table I; the air bubble is bound by two planes, both parallel to the shock front and 2.4 mm apart. Figure 1 shows a time series for this simulation. The final image exhibits an expansion shock that is qualitatively similar to that in Fig. 4.

6.2. Shock–Bubble Interaction: One Bubble

A simulation of a shock interacting with a cylindrical bubble of diameter 6 mm is now given; the fluid properties are as above. These simulations differ from Ivings' in that they continue beyond the point at which the shock leaves the bubble.

Figure 2 shows the bubble just before the shock hits it (signals cannot travel faster than the shock speed, so the bubble is undisturbed) and at three subsequent times. Note that the shock remains relatively sharp (the shock is four to five computational fluid elements wide, a value typical of Flux Correction [35]) which itself gives confidence in the numerical scheme.

The backward-moving rarefaction shock (as predicted by Grove and Menikoff [9] and, numerically, by Ivings [14]) is clearly visible in the second and third diagrams of Fig. 2 as an expanding ring. In the fourth diagram, the bubble has split into two as a liquid jet is formed, in agreement with the experimental findings of Bourne and Field [1].

Note that disturbances propagate more slowly inside the bubble than in water; thus the shock front is retarded by the bubble. However, the liquid jet does initiate a shock wave in the undisturbed water that may be seen in the fourth diagram.

Figures 3 and 4 show, in perspective form, the density of the computational domain about 2.2 μs and 5.6 μs after the shock hit the bubble. Comparing these figures shows that the shock propagates at a speed of about 2944 m/s.

TABLE I
Shock–Bubble Interaction: Initial Conditions, Following Sugimura *et al.* [29]

	Density (kg/m^3)	Speed (m/s)	Pressure (Pa)	γ	Stagnation energy (J/m^3)
Post-shock	1225.6	542.76	1.6×10^9	7.15	794.2×10^6
Gas bubble	1.2	0	101325	1.4	253.3×10^3
Pre-shock	1000	0	101325	7.15	353.4×10^6

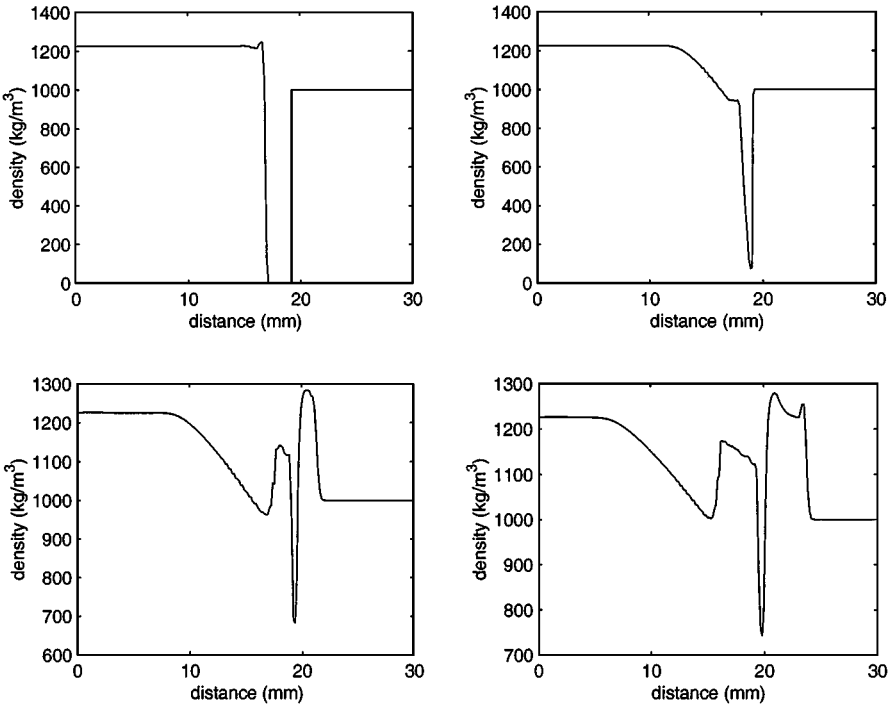

FIG. 1. Shock–bubble interaction for a planar bubble. Density as a function of position just after shock reaches the bubble; and after 1.4, 2.6, and 3.4 μs. Undisturbed bubble thickness 2.4 mm.

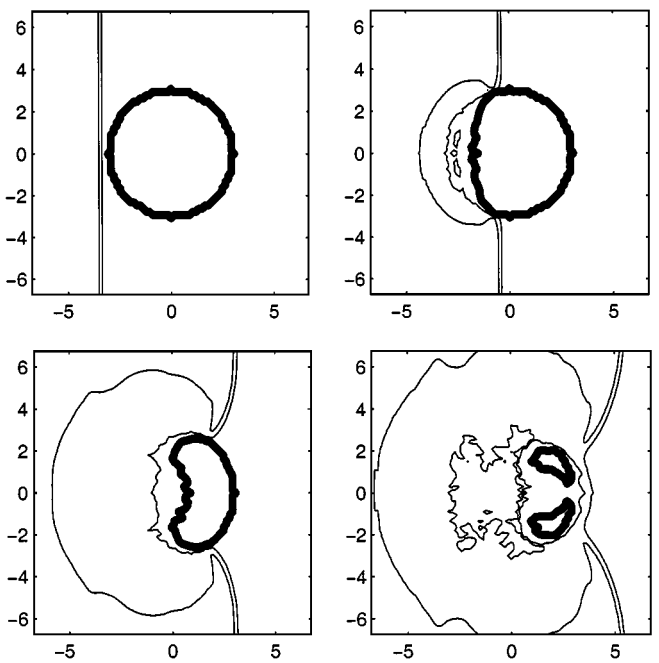

FIG. 2. Shock–bubble interaction just after shock reaches bubble; and after 1.0, 2.2, and 3.0 μs. Thin lines show water density contours (1150 and 1050 kg/m^3) and the thick line shows the meniscus. Undisturbed bubble diameter 6 mm; axes show distance from bubble center in mm.

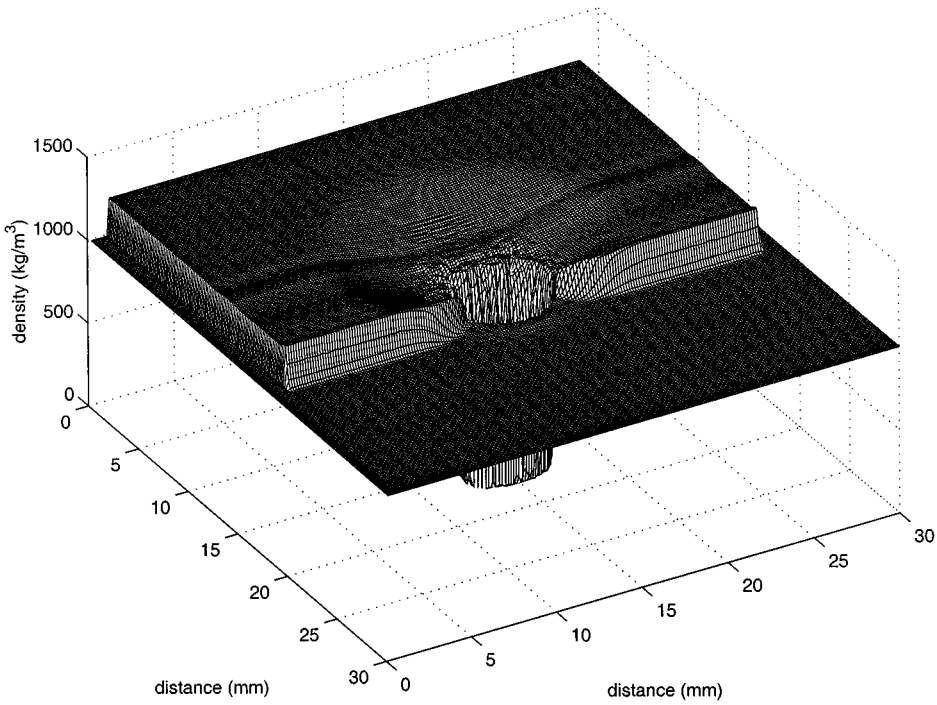

FIG. 3. Numerical solution of shock–bubble interaction 2.2 μs after shock hits bubble; meshplot of density. Original bubble diameter 6 mm.

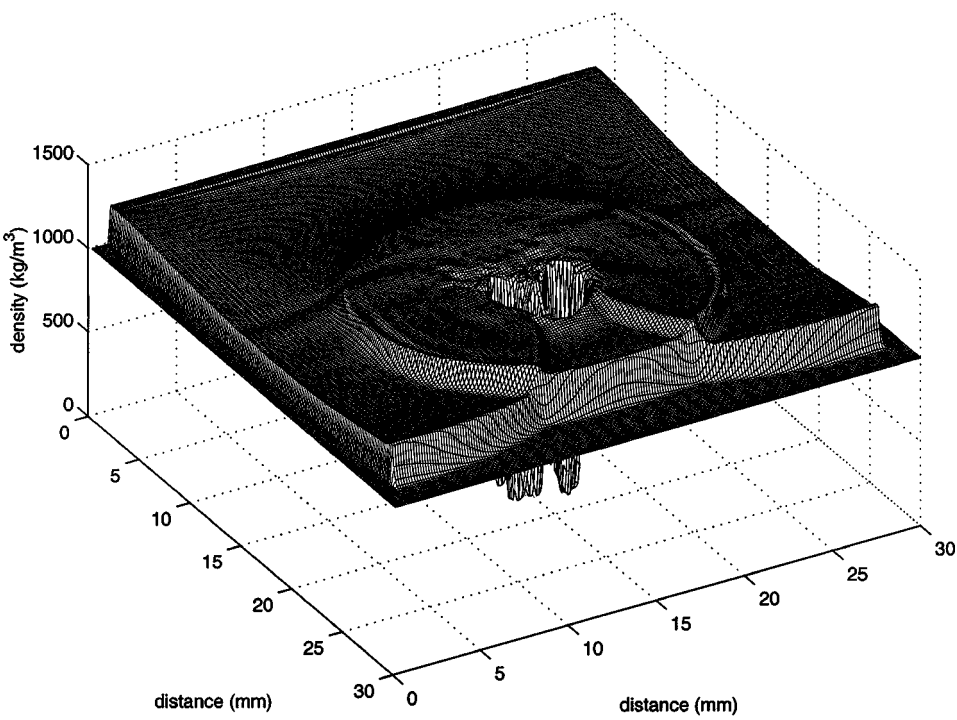

FIG. 4. Numerical solution of shock–bubble interaction 5.6 μs after shock hits bubble; meshplot of density. Original bubble diameter 6 mm.

Figure 3 shows the rarefaction shock propagating away from the bubble. At this stage, the bubble is still collapsing and the water immediately behind the bubble is moving faster than the following flow but slower than the shock speed. It is the case that within the rarefaction shock region, the velocity has a transverse component that acts to focus both kinetic and internal energy in the vicinity of the bubble.

In Fig. 4, an almost axisymmetric shock propagates away from the air bubble as it expands. The energy driving this process is derived from the energy focused by the rarefaction shock. The original shock front has almost returned to its equilibrium, planar form to which it tends asymptotically.

The two points at which the expansion shock intersects the reforming original shock are of particular interest. At these points, undisturbed fluid (in this case water) is interacting with the two shocks simultaneously and the small but finite thicknesses of the simulated shocks are clearly visible.

6.3. Two Bubbles

Because the methods presented in this paper do not have to track changes in topology of the meniscus, it is possible to simulate arbitrary configurations of air and water in the computational domain.

Figures 5 and 6 show a shock interacting with two air bubbles of diameters 6 and 3 mm. This simulation illustrates the complex interactions that can occur; in Fig. 6, the larger bubble is still in the rarefaction shock phase while the smaller bubble has reached the expansion shock phase.

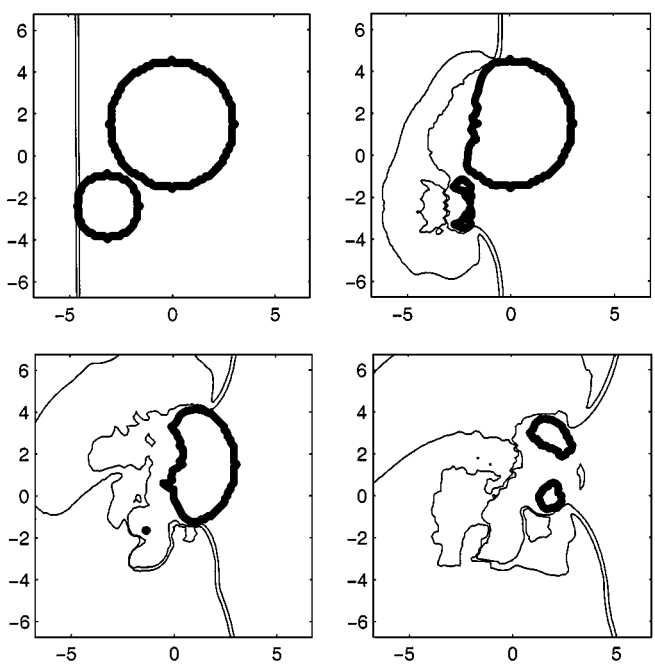

FIG. 5. Shock–bubble interaction just after shock reaches smaller bubble; and after 1.4, 2.6, and 3.4 μs. Thin lines show water density contours (1150 and 1050 kg/m^3) and the thick line shows the meniscus bounding the circular air bubble. Undisturbed bubble diameters 3 mm and 6 mm.

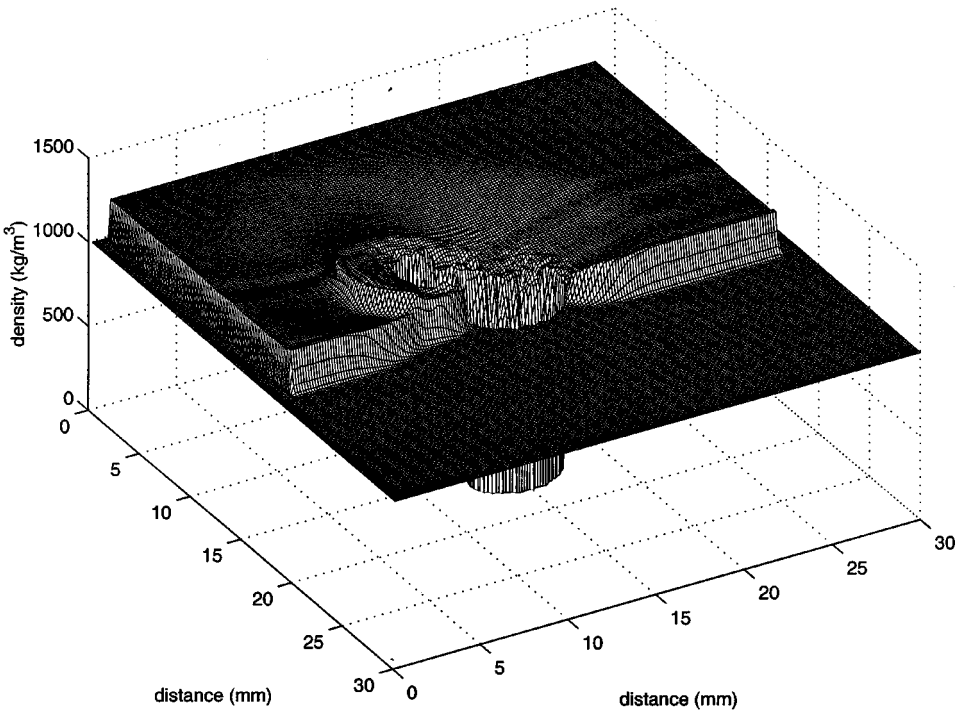

FIG. 6. Numerical solution of a shock interacting with two bubbles after 2.6 μs; meshplot of density. Original bubble diameters 6 mm and 3 mm.

In Fig. 5, the smaller bubble apparently disappears; this is because its size becomes comparable to the dimensions of the numerical grid. In the simulations presented here, mass of air is conserved to within one part in 10^4.

6.4. A Foam Bubble

We now consider the original (single) bubble problem but replace the air bubble with a foam comprising 50% water and 50% air by volume, as described in Table II.

Such a foam bubble has very different properties from an air bubble: its density is about 500 kg/m^3 (as opposed to 1.2); it is less compressible than air; and sound travels at a speed different from that of either pure air or pure water (the exact value depends on the pressure).

Figure 7 shows simulation of a shock wave in water interacting with a small region comprising 50% air by volume. The shock, originally planar, is deflected by the presence

TABLE II
Shock–Foam Bubble Interaction: Initial Conditions

	Density (kg/m^3)	Speed (m/s)	Pressure (Pa)	γ	Stagnation energy (J/m^3)
Post-shock	1225.6	542.76	1.6×10^9	7.15	794.2×10^6
Foam bubble	500.6	0	101325	n/a	176.9×10^6
Pre-shock	1000	0	101325	7.15	353.4×10^6

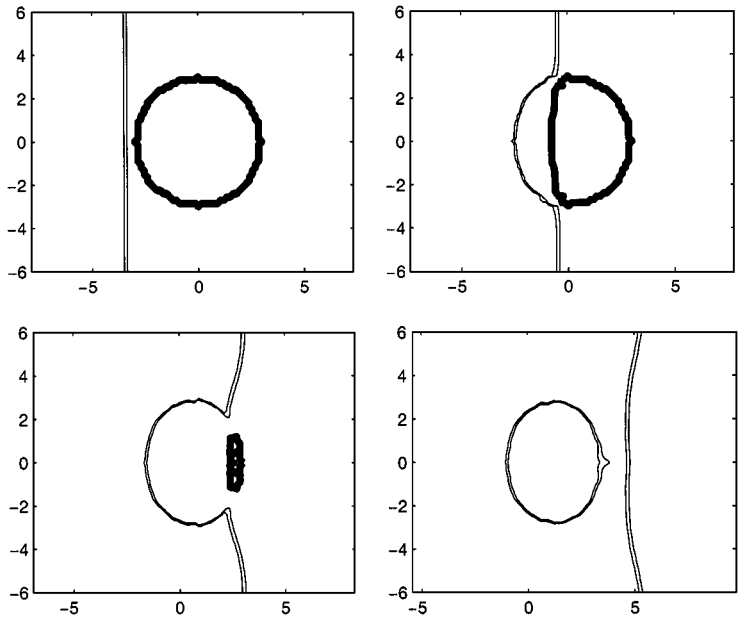

FIG. 7. Shock–bubble interaction just after shock reaches (50% by volume) foam bubble; and after 1.0, 2.2, and 3.0 μs. Thin lines show water density contours (1150 and 1050 kg/m^3) and the thick line shows the boundary of the circular foam bubble. Undisturbed bubble diameter 6 mm.

of the foam, but not to the extent seen in Fig. 2. There is less distortion of the inclusion's outline, and the rarefaction shock is much weaker. Also note how the meniscus disappears in the fourth frame: this is because the thick line is the contour corresponding to volume fraction $\nu = 0.5$, and the foam region is subject to higher than atmospheric pressure after the passage of the shock. This preferentially compresses the air leading to a higher volume fraction. The contour line is absent because nowhere in the computational domain does the volume fraction exceed 0.5.

Some of these results might be expected because of the inclusion's intermediate density (500 kg/m^3) and compressibility although the detailed structure of the flow is not amenable to simple analysis.

7. CONCLUSIONS AND FURTHER WORK

This paper has developed a new equation of state that gives the pressure of a gas–water mixture in terms of variables that obey conservation equations. Thus, compressible flow in two media may be simulated.

Although the primary goal of this work was to simulate shock–bubble interactions (the new EOS being required to handle computational elements through which a meniscus passes), applications of this work might include the simulation of shocks moving through foams and droplet-laden gas. This is straightforward in principle, although further work would be required to determine a multiphase generalization of Table I.

Further work might include extension of the present computational method to three dimensions. Applications of the present work include simulation of problems in shock wave lithotripsy, explosive detonation, and compressible flow in bubbly fluids.

REFERENCES

1. N. K. Bourne and J. E. Field, Shock-induced collapse of single cavities in liquids, *J. Fluid Mech.* **244**, 225 (1992).
2. A. W. Campbell, W. C. Davis, and J. R. Travis, Shock initiation of detonation in liquid explosives, *Phys. Fluid* **4**(4), 498 (1961).
3. G. F. Carrier, Shock waves in a dusty gas, *J. Fluid Mech.* **4**, 376 (1958).
4. D. P. Chock, A comparison of numerical methods for solving the advection equation, part 2, *Atmos. Environ.* **19**(4), 571 (1985).
5. J. F. Clarke *et al.*, Numerical computation of two-dimensional unsteady detonation waves in high-energy solids, *J. Comput. Phys.* **106**, 215 (1993).
6. M. Delius *et al.*, Extracorporeal shock waves act by shock wave-gas bubble interaction, *Ultrasound Med. Biol.* **24**(7), 1055 (1998).
7. Zhong Ding and S. M. Gracewski, The behaviour of a gas cavity impacted by a weak or strong shock wave, *J. Fluid Mech.* **309**, 183 (1996).
8. R. P. Fedkiw, T. Anslam, B. Merriman, and S. Osher, A non-oscillatory Eulerian approach to interfaces in multimaterial flows (the ghost fluid method), *J. Comput. Phys.* **152**, 457 (1999).
9. J. W. Grove and R. Menikoff, Anomalous reflection of a shock wave at a fluid interface, *J. Fluid Mech.* **219**, 313 (1990).
10. R. K. S. Hankin, *Heavy Gas Dispersion Over Complex Terrain*, Ph.D. thesis (Cambridge University, 1997).
11. R. K. S. Hankin, *LIQUIDEE: Modelling of Bund Overtopping*, Technical Report CMS/98/06 (Health and Safety Laboratory, Harpur Hill, Buxton, Derbyshire SK17 9JN, 1998).
12. R. K. S. Hankin and R. E. Britter, TWODEE: the Health and Safety Laboratory's shallow layer model for dense gas dispersion-Part 1, mathematical basis and physical assumptions, *J. Hazardous Mater.* **66**(3), 211 (1999).
13. C. W. Hirt, Heuristic stability for finite-difference equations, *J. Comput. Phys.* **2**, 39 (1968).
14. M. J. Ivings, Wave propagation through gases and liquids, Ph.D. Thesis, Manchester Metropolitan University (1997).
15. P. Jenny *et al.*, Correction of conservative Euler solvers for gas mixtures, *J. Comput. Phys.* **132**, 91 (1997).
16. M. Kameda and Y. Matsumoto, Shock waves in a liquid containing small gas bubbles, *Phys. Fluids* **8**(2), 322 (1996).
17. S. Karni, Multicomponent flow calculations by a consistent primitive algorithm, *J. Comput. Phys.* **112**(1), 31 (1994).
18. S. Karni, Hybrid multifluid algorithms, *SIAM J. Sci. Comput.* **17**(5), 1019 (1996).
19. T. Kodama and K. Takayhama, Dynamic behavior of bubbles during extracorporeal shock-wave lithotripsy, *Ultrasound Med. Biol.* **24**(5), 723 (1998).
20. P. Mazel, R. Saurel, J.-C. Lorand, and P. B. Butler, A numerical study of weak shock wave propagation in a reactive bubbly liquid, *Shock Waves* **6**, 287 (1996).
21. R. Menikoff and B. J. Plohr, Riemann problem for fluid flow of real materials, *Rev. Mod. Phys.* **61**(1), 75 (1989).
22. J. Mulder, S. Osher, and J. A. Sethian, Computing interface motion in compressible gas dynamics, *J. Comput. Phys.* **100**, 209 (1992).
23. M. Olim, M. E. H. Van Dongen, T. Kitamura, and K. T. Takayama, Numerical simulation of the propagation of shock waves in open-cell porous foams, *Int. J. Multiphase Flow* **20**(3), 557 (1994).
24. J. Pike, Analytic solutions for dusty shock waves, *Am. Inst. Aeronaut. Astronaut.* **32**(5), 979 (1994).
25. P. J. Roache, *Computational Fluid Dynamics* (Hermosa, Albuquerque, NM, 1982).
26. R. Saurel and R. Abgrall, A multiphase Godunov method for compressible multifluid and multiphase flows, *J. Comput. Phys.* **150**, 425 (1999).
27. R. Saurel and R. Abgrall, A simple method for compressible multifluid flows, *SIAM J. Sci. Comput.* **21**, 1115 (1999).

28. K.-M. Shyue, An efficient shock-capturing algorithm for compressible multicomponent problems, *J. Comput. Phys*. **142**, 208 (1998).
29. T. Sugimura, K. Tokita, and T. Fujiwara, Nonsteady shock wave propagating in a bubble-liquid system, *Report Fac. Sci. Tech. Meijo Univ (Japan)* **24**, 67 (1984).
30. M. J. Tan and S. G. Bankoff, Propagation of pressure waves in bubbly mixtures, *Phys. Fluids* **27**(6), 1362 (1984).
31. V. T. Ton, Improved shock-capturing methods for multicomponent and reacting flows, *J. Comput. Phys*. **128**, 237 (1996).
32. M. Watanabe and A. Prosperetti, Shock waves in dilute bubbly liquids, *J. Fluid Mech*. **274**, 349 (1994).
33. P. Woodward and P. Colella, The numerical simulation of two-dimensional fluid flow with strong shocks (review article), *J. Comput. Phys*. **54**, 115 (1984).
34. J. B. Young, The fundamental equations of gas-droplet multiphase flow, *Int. J. Multiphase Flow* **21**(2), 75 (1995).
35. S. T. Zalesak, Fully multidimensional flux-corrected transport algorithms for fluids, *J. Comput. Phys*. **31**, 335 (1979).
36. S. T. Zalesak, High order "ZIP" differencing of convective terms, *J. Comput. Phys*. **40**, 497 (1981).